ACI STRUCTURAL JOURNAL TECHNICAL PAPER

Title no. 108-S13

Design of Large Footings for One-Way Shear

by Almila Uzel, Bogdan Podgorniak, Evan C. Bentz, and Michael P. Collins

Because ACI design procedures do not account for the size effect in shear, there is concern that these procedures may be unconservative for large concrete footings not containing shear reinforcement. This paper describes an experimental program involving 16 specimens designed to investigate the one-way shear strength of footings of different thicknesses, slenderness ratios, and applied loading patterns. Analytical studies were also performed to evaluate the accuracy of currently available design procedures. It was found that a combination of sectional models to predict the flexural and shear capacities of slender footings and strut-and-tie models to predict the shear capacity of footings with low slenderness ratios gave accurate results.

Keywords: footings; shear; size effect; strut-and-tie; uniformly loaded members.

INTRODUCTION

Reinforced concrete footings such as those shown in Fig. 1 are usually constructed without shear reinforcement and hence the thickness of these footings is often governed by the concrete contribution to shear strength V_c. For footings, ACI 318-08[1] requires that the shear strength be checked for both "beam action shear," (that is, one-way shear) and "two-way action shear" (that is, punching shear). As shown in Fig. 1, the specified critical section for beam action shear is located in a plane across the entire width of the footing. In the design of high-rise buildings, large column or wall loads can sometimes result in the need for footings more than 10 ft (3 m) thick.

When the ACI shear provisions were developed,[2-4] it was not appreciated that the failure shear stress for slender members not containing shear reinforcement decreases as the thickness of the structural member increases.[5-8] Because ACI 318-08[1] does not account for this size effect, concern has been expressed regarding the safety of very thick footings.[8] Richart,[9-10] in his classic 1948 footings papers, noted that "the factor of safety of thin footings… appears greater than in thick footings." Although the footings shown in Fig. 1 can be very thick, the ratio of their tributary shear length L_0 to their effective depth d is typically not very large. When this ratio is low, an alternate force-resisting mechanism consisting of diagonal struts and tension ties can form, and this may provide adequate shear resistance even for very thick footings.

This paper will describe a series of experiments designed to investigate the one-way shear strength of large footings. In addition, the results of analytical studies using strut-and-tie models will be used to determine situations in which the current ACI shear provisions are of adequate safety. Finally, some suggested modifications to ACI 318-08[1] will be presented.

RESEARCH SIGNIFICANCE

The experiments and the associated analytical studies in this paper provide new information on the safety of footings designed by ACI 318-08.[1] Code modifications are recommended that would limit the potential for unsafe shear designs of large footings not containing shear reinforcement.

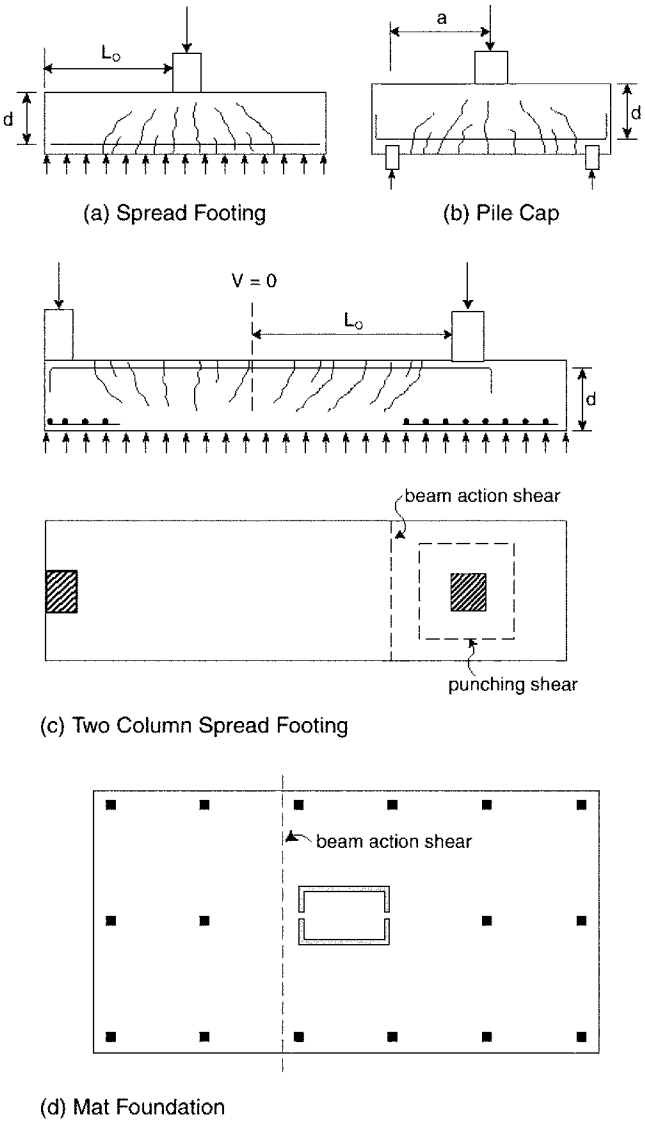

Fig. 1—Examples of large footings.

SIZE EFFECT IN SHEAR

Figure 2 illustrates the size effect in shear for two major series of simple span specimens. The U series[7] consists of uniformly loaded members, whereas the P series[11] consists

ACI Structural Journal, V. 108, No. 2, March-April 2011.
MS No. S-2006-397.R4 received May 9, 2010, and reviewed under Institute publication policies. Pertinent discussion including author's closure, if any, will be published in the January-February 2012 *ACI Structural Journal* if the discussion is received by September 1, 2011.

Almila Uzel *is a Structural Engineer with Halcrow Yolles in Toronto, ON, Canada. She received her PhD from the University of Toronto, Toronto, ON, Canada.*

Bogdan Podgorniak *is a Principal of Podgorniak Structural Engineering Inc. in Burlington, Canada, and was previously a Design Engineer with Leslie E. Robertson Associates. He received his MASc from the University of Toronto.*

Evan C. Bentz, *FACI, is an Associate Professor of Civil Engineering at the University of Toronto and is a member of Joint ACI-ASCE Committee 445, Shear and Torsion.*

Michael P. Collins, *FACI, is a University Professor and Bahen-Tanenbaum Professor of Civil Engineering at the University of Toronto. He is a member of Joint ACI-ASCE Committee 445, Shear and Torsion.*

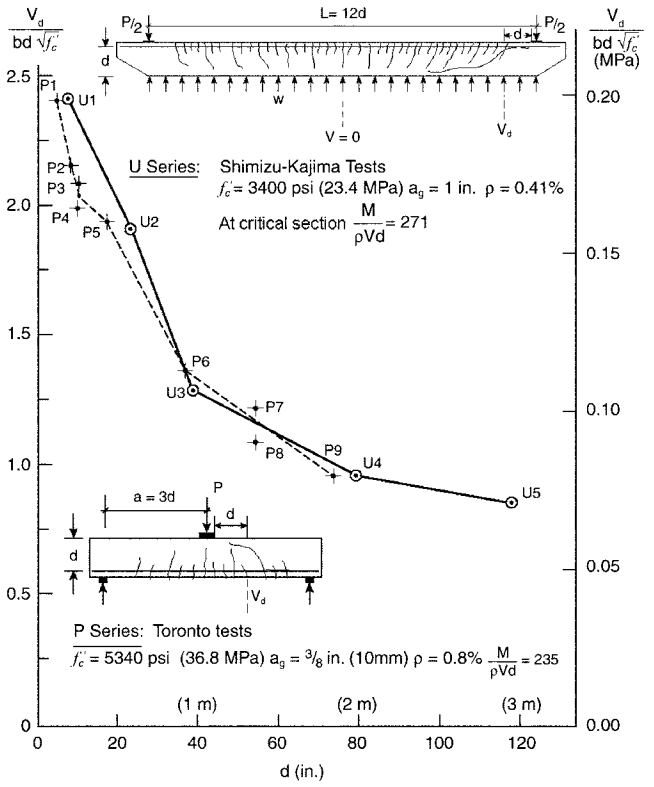

Fig. 2—Experimental results illustrating size effect in shear.

of point-loaded members. The basic ACI expression for the failure shear stress v of a member without shear reinforcement is given by

$$v = \frac{V_c}{bd} = 1.9\sqrt{f_c'} + 2500\rho\frac{Vd}{M} \le 3.5\sqrt{f_c'} \quad \text{(psi units)} \quad (1)$$

Joint ACI-ASCE Committee 326,[2-4] which developed this expression, chose the parameter $M/(\rho Vd)$ because the stress in the longitudinal reinforcement f_s at shear failure is directly proportional to this parameter and it was observed that v decreased as f_s increased. The committee recommended that $M/(\rho Vd)$ be calculated at the critical section for shear, taken as d from a point load, or for uniformly loaded beams, d from the reaction area. It can be seen from Fig. 2 that these two series of slender beams, which have similar values of $M/(\rho Vd)$ at the critical sections for shear, have very similar failure shear stresses. However, rather than v remaining constant as d increases, which the ACI expression predicts, the failure shear stress systematically reduces as d increases, which is called the size effect in shear.

The simplest explanation of the size effect in shear is that the larger flexural crack widths that occur in larger members reduce the aggregate interlock capacity of these cracks and hence trigger failure at lower shear stresses.[11] Crack widths near middepth where the shear stress is high increase nearly linearly with both the tensile strain in the longitudinal reinforcement and the spacing between cracks. This spacing, in turn, has been shown[7] to be proportional to member depth. The shear stress that can be transmitted across such cracks, however, decreases as the crack width increases and as the nominal maximum coarse aggregate size a_g decreases.[12] Based on this reasoning, the simplified equations[13] of the modified compression field theory (MCFT)[14] for sectional shear strength have a first term in the denominator that models the strain effect and a second term that models the size effect. These equations are incorporated in CSA A23.3-04[15]

$$v = \frac{V_c}{bd} = \frac{220\sqrt{f_c'}}{(1 + 1500\varepsilon_x)(39 + s_{xe})} \quad \text{(psi, in.)} \quad (2)$$

where the effective crack spacing s_{xe} is given by

$$s_{xe} = 1.24d/(a_g + 0.63) \ge 0.75d \quad \text{(in. units)} \quad (3)$$

The longitudinal strain at middepth, ε_x, for reinforced concrete members not subjected to axial load is calculated by

$$\varepsilon_x = v \times \frac{1 + 1.11\dfrac{M}{Vd}}{2E_s\rho} \quad (4)$$

To use these CSA A23.3-04[15] equations, the two unknowns, v and ε_x, are found from Eq. (2) and (4). If these equations are used to calculate the failure shear stress of the 14 test results shown in Fig. 2, the ratios of the measured-to-calculated shear stresses have an average value of 1.07, a coefficient of variation (COV) of 12.1%, and a least conservative value of 0.87. On the other hand, because the basic ACI 318-08[1] equation does not account for the size effect, its average value of the test-to-predicted ratios is 0.79, the COV is 34.8%, and the least conservative value is 0.42.

SLENDERNESS EFFECT IN SHEAR

The two series of experiments shown in Fig. 2 not only had very similar failure shear stresses at similar depths, but also showed similar behavior when they failed in shear, in that they failed soon after the formation of the first significant diagonal crack. For shorter members with small slenderness ratios, shear failures do not typically occur upon the formation of the first significant diagonal crack. Rather, the internal forces in the member redistribute from those associated with beam action to those associated with arch action, enabling the member to carry even higher loads. The capacity of this "remaining arch"[16] can be determined using a strut-and-tie model. Thus, the shear capacity of the member can be taken as the larger of that from the sectional model, which predicts the breakdown of beam action, and the strut-and-tie model, which predicts the capacity of the remaining arch. All of the beams shown in Fig. 2 are sufficiently slender such that the capacity of the remaining arch is less than the shear corresponding to the breakdown of beam action and hence they fail upon the occurrence of the first significant diagonal crack.

Numerous series of shear tests[16-18] have shown that as the slenderness of a beam decreases, the shear stress at failure increases. Figure 3 shows the results of two such series of simply supported beams tested at the University of Stuttgart.[17] The P series had 17 beams subjected to point loads in which the shear span-depth ratio (a/d) varied from 1 to 8. The U series had 14 beams subjected to uniformly distributed loads in which L/d varied from 5 to 22. The beams all had similar cross-sectional dimensions and material properties. Kani[19] suggested that in comparing uniformly loaded beams with point-loaded beams, the uniform load on each half of the span should be replaced by a point load at the quarter point of the span because such an equivalent point load causes the same shear at the reaction and the same midspan moment. This procedure has been used in preparing Fig. 3, which also shows the corresponding strut-and-tie model used for these equivalent point loads. To be consistent with this procedure, the vertical axis in Fig. 3 uses the shear at the support rather than the shear at the critical section, whereas the horizontal axis uses either a/d or $0.25L/d$. With these chosen axes, neither the flexural failure strength nor the predicted strut-and-tie shear strength depend on the type of loading. Thus, there is only one line on the plot for each of these failure modes. The predictions for the beam action failure shears shown in Fig. 3 were determined from the simplified MCFT equations (Eq. (2) through (4)) and different predictions for the shear at the support are obtained for the P and U type beam shear failures. This is because for the P series, the critical section is near the load, which has high moments, and the shear at this location is essentially the same as that at the support. For the U series, however, the critical section is d from the support, where the moment is low, and the shear at the support can be significantly higher than the shear at this critical section.

The provisions of the AASHTO LRFD specifications[20] were used to generate the strut-and-tie predictions shown in Fig. 3. Although these provisions are similar to those of ACI 318-08[1] Appendix A, they provide a more general and accurate procedure for estimating the failure strength of the critical diagonal strut.[11] ACI 318-08[1] assumes that a diagonal strut such as that shown in Fig. 3 will fail when the compressive stress reaches $0.85 \times 0.6f_c'$. The AASHTO LRFD provisions,[20] which are based on the MCFT,[14] give the failure stress of this strut, f_{ce}, as

$$f_{ce} = \frac{f_c'}{0.8 + 170\varepsilon_1} < 0.85f_c' \tag{5}$$

where the principal tensile strain ε_1 in the concrete perpendicular to the strut is

$$\varepsilon_1 = \varepsilon_s + (\varepsilon_s + 0.002)\cot^2\alpha_s \tag{6}$$

In this equation, ε_s is the calculated strain in the reinforcement at the failure load, whereas α_s is the angle between the compressive strut and the reinforcement (refer to Fig. 3). As Eq. (5) indicates that the strut strength will be lowest where the longitudinal tensile straining is greatest, the calculated critical strength in the strut will be that calculated at the flexural tension side of the member. Also note that for low angles of α_s, the $\cot^2\alpha_s$ term becomes very large and thus f_{ce} becomes very low.

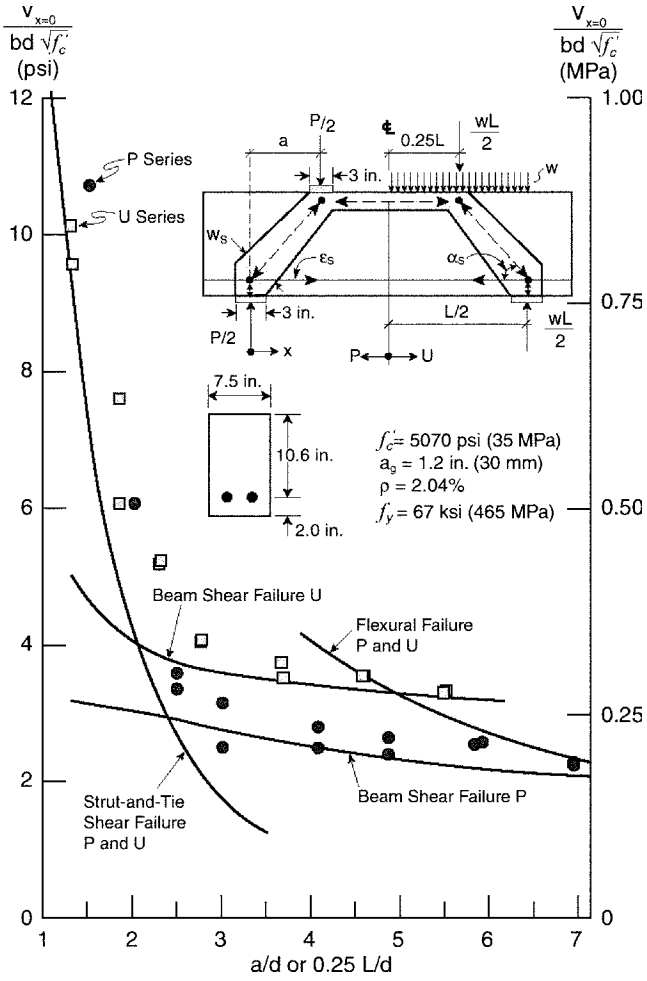

Fig. 3—Predicted and observed failure loads for Stuttgart point-loaded (P) and uniformly loaded (U) beams.

For both the ACI 318-08[1] and AASHTO LRFD[20] strut-and-tie methods, the width of the strut w_s shown in Fig. 3 is calculated as

$$w_s = \ell_b \sin\alpha_s + w_t \cos\alpha_s \tag{7}$$

where ℓ_b is the length of the bearing plate, and w_t is the effective height of concrete concentric with the reinforcing tie, which can be taken as $2 \times (h - d)$.

The strut-and-tie predicted failure loads shown in Fig. 3 were obtained by optimizing the geometry of the model to maximize the predicted failure load. This involved finding the depth of the top horizontal strut so that its stress at failure equaled $0.85f_c'$ and determining the applied load that caused the compressive stress in the diagonal strut to equal f_{ce}. Note that, unlike the predicted sectional shear strengths, the predicted strut-and-tie shear strengths do not have a size effect, as the concrete is predicted to fail at the same compressive stress irrespective of the size of the member. It can be seen from Fig. 3 that the strut-and-tie predictions follow the trend of the experimental results very well. It can also be seen that if the shear strength predictions are based only on the beam action sectional failure shears, the strength of members with low slenderness ratios will be grossly underestimated. Combining the predictions for the flexural, sectional shear, and strut shear strengths, the average value

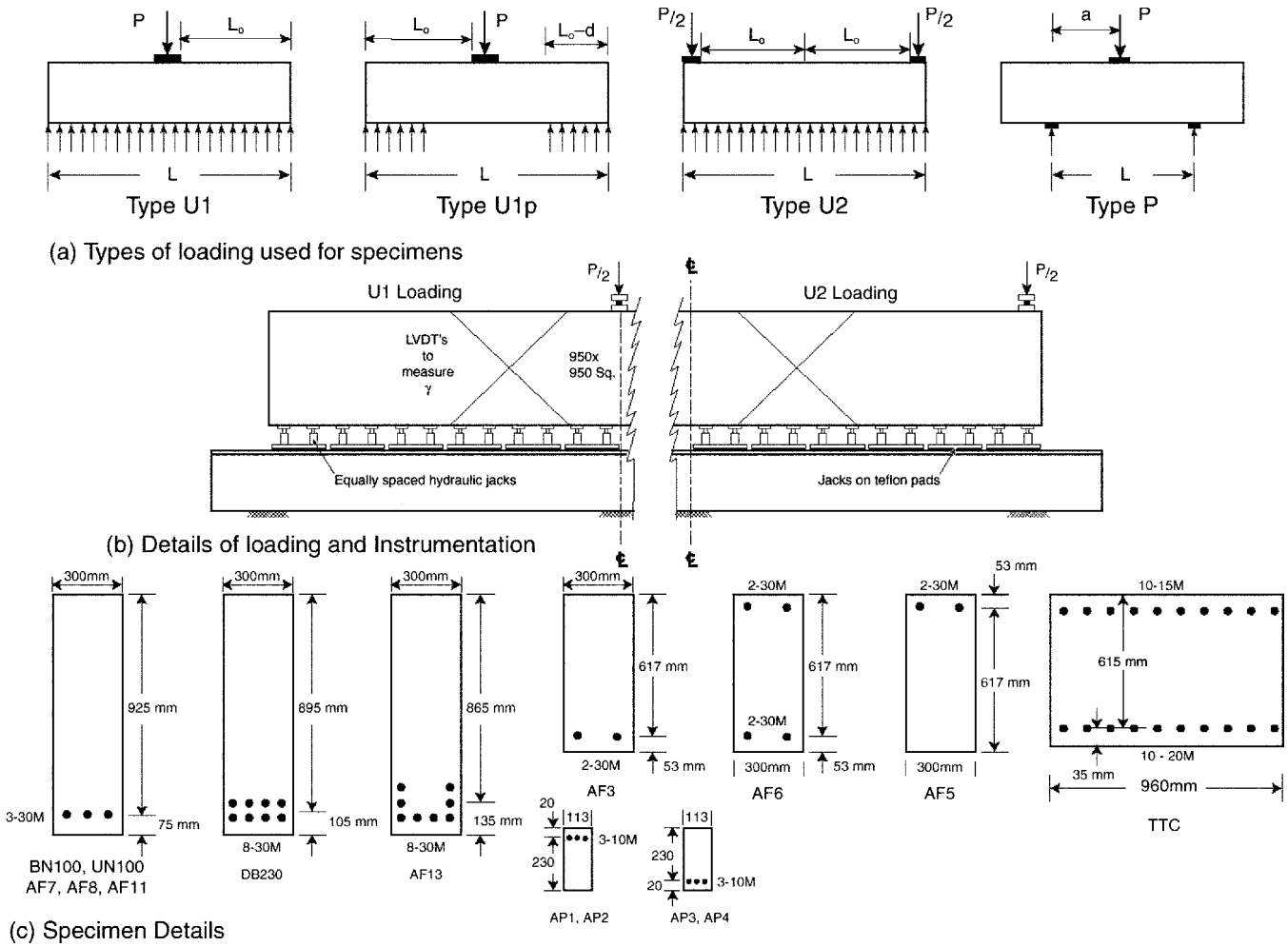

Fig. 4—Details of experimental program. (Note: 1 in. = 25.4 mm.)

of the ratio of experimental-to-predicted strength for the 31 specimens is 1.16, the COV is 12.6%, and the least conservative ratio is 0.89.

If the members summarized in Fig. 3 are analyzed by the ACI basic shear strength equation (Eq. (1)) and the ACI 318-08[1] Appendix A strut-and-tie provisions, the average ratio of experimental-to-predicted shear strength is 1.21 and the COV is 15.4%, while the least conservative ratio is 0.78. The AASHTO LRFD[20] strut-and-tie predicted strengths shown in Fig. 3 decrease in a continuous curve as the slenderness increases. The ACI 318-08[1] predicted strut-and-tie strengths, which are not shown, decrease more gradually until an a/d of approximately 1.85, after which point no ACI strut-and-tie predictions are possible because of the ACI requirement that α_s not be taken less than 25 degrees. One reason for this limit is that for lower angles, the ACI-predicted strut strength becomes increasingly unconservative.[21]

EXPERIMENTAL PROGRAM

To investigate safety concerns with large, lightly reinforced footings, a series of tests was performed on specimens with effective depths d up to 3 ft (1 m). Specimens representing a 1 ft (300 mm) wide footing strip were tested under either concentrated loads or uniformly distributed loads (refer to Fig. 4(a)). Table 1 summarizes these 13 new tests,[22] along with three previously published (BN100, DB230, and TTC) Toronto results[8,23] and the eight large footings tested by Richart,[9-10] for which one-way shear was critical. Richart's[9-10] specimens were loaded by 14 x 14 in. (356 x 356 mm) columns and were supported on a bed of springs. The first eight Toronto tests in Table 1 are large-scale specimens with effective depths of approximately 3 ft (1 m) (refer to Fig. 4(c)). The next four tests are intermediate-scale specimens with effective depths of approximately 2 ft (600 mm), while the final four tests are small-scale specimens with effective depths of approximately 9 in. (230 mm). Straight reinforcing bars extending to the ends of the specimens were used in all of the Toronto tests.

Loading designations U1, U2, U1p, and P are used in Table 1 to identify the type of loading applied to the specimens, and these loading types are described in Fig. 4(a). The small-scale specimens were loaded with an oil-filled rubber bag between the specimen and the bed of the testing machine. The top reaction was provided by a plate 6 in. (150 mm) wide in the span direction, supported by rollers and reacting against the head of the testing machine. For the large-scale specimens, the uniformly distributed load was produced by a large number of small hydraulic jacks supplied by a single manifold,[22] as shown in Fig. 4(b). The jack forces were applied to the specimens through 4 x 4 x 1 in. (100 x 100 x 25 mm) bearing plates. Each bearing plate sat on the spherical seat attached to the ram of the jack. The base of each jack was positioned on a steel plate and two layers of 1/8 in. (3 mm) lubricated polytetrafluoroethylene sheets

Table 1—Experimental observations and predictions for footing specimens

									Experimental observations						Predictions					
Name	Load type	L, in.	L_0/d or a/d	f_c', psi	a_g, in.	ρ, %	f_y, ksi	$\frac{M}{\rho V d}$	P_{fail}, kips	$2\Delta/L$, $\times 10^{-3}$	γ, $\times 10^{-3}$	w, mm	ε_s, $\times 10^{-3}$	$\frac{V_d}{bd\sqrt{f_c'}}$	α_s, deg	ε_x, $\times 10^{-3}$	$V_d/(bd\sqrt{f_c'})$, psi Flex	Strut	Beam	Exp./Pred.
Richart footing specimens, 1948; d = 16 in.																				
502a	U1	108	2.94	3530	1	0.54	60.9	180	554	—	—	—	2.5	2.33	18.2	0.78	**2.04**	2.14	1.98	1.14
502b	U1	108	2.94	3285	1	0.54	60.9	180	578	—	—	—	2.5	2.51	18.1	0.76	2.10	**2.09**	2.00	1.20
503a	U1	108	2.94	3545	1	0.54	60.9	180	586	—	—	—	2.5	2.46	18.2	0.78	**2.04**	2.14	1.98	1.21
503b	U1	108	2.94	3480	1	0.54	60.9	180	550	—	—	—	2.5	2.33	18.2	0.78	**2.05**	2.13	1.98	1.14
505a	U1	120	3.31	3680	1	0.68	61.6	170	549	—	—	—	2.3	2.90	16.4	0.73	2.39	1.90	**2.06**	1.41
505b	U1	120	3.31	3730	1	0.68	61.6	170	525	—	—	—	2.3	2.76	16.4	0.73	2.38	1.91	**2.05**	1.35
505a	U1	120	3.31	3350	1	0.68	61.6	170	500	—	—	—	2.3	2.78	16.4	0.70	2.49	1.84	**2.09**	1.33
506b	U1	120	3.31	3810	1	0.68	61.6	170	500	—	—	—	2.3	2.60	16.4	0.73	2.38	1.93	**2.04**	1.27
Large-scale specimens, present study; d = 36.4 in. (d = 35.2 in. for DB230, d = 34.1 in. for AF13)																				
BN100	P	213	2.92	5370	3/8	0.76	79.8	243	83	2.2	0.6	0.30	1.2	1.37	18.8	0.67	2.64	0.90	**1.32**	1.04
UN100	U1	236	3.16	6230	3/8	0.76	79.8	143	267	3.9	3.1	2.00	2.0	2.61	17.9	0.57	3.04	**2.91**	1.43	0.90
AF7	U1p	236	3.16	4900	3/4	0.76	81.5	143	160	3.9	2.6	2.50	1.82	2.71	17.8	0.58	3.85	**2.68**	1.65	1.01
AF8	P	157	2.16	4900	3/4	0.76	81.5	143	109	2.9	1.4	1.10	1.38	1.86	24.5	0.58	3.85	**1.72**	1.65	1.08
AF11	U1	157	2.00	5250	3/4	0.76	81.5	66	595	5.5	2.4	1.40	9.7	4.41	25.8	0.47	**3.67**	4.28	1.81	1.20
AF11-r	U1p	157	2.00	5250	3/4	0.76	81.5	66	317	4.7	2.6	2.00	2.0*	4.75	25.8	0.47	4.76	**4.28**	1.81	1.11
DB230	P	213	3.02	4640	3/8	2.09	79.8	91	113	2.0	1.2	0.90	0.8	2.04	18.0	0.32	6.39	1.22	**1.83**	1.11
AF13	U1	236	3.38	5180	3/4	2.16	68.9	55	418	4.1	3.2	2.00	1.4	4.95	19.6	0.29	6.97	**4.05**†	2.20	1.22
Intermediate-scale specimens, present study; d = 24.3 in.																				
AF3	U1	236	4.74	3960	3/4	0.76	68.9	247	122	5.1	1.8	1.15	2.6	2.59	12.4	0.75	2.48	1.19	**1.70**	1.52
AF5	U2	236	4.54	4540	3/4	0.76	68.9	180	124	8.1	2.3	0.40	2.6	2.34	22.5	0.68	2.35	1.20	**1.80**	1.30
AF6	U1	236	2.94	4670	3/4	0.76	81.5	128	292	7.9	3.4	1.40	2.1	2.97	18.9	0.61	3.59	**2.87**	1.89	1.03
TTC	U2	216	3.90	6520	3/8	0.51	71.1	261	411	4.6	1.4	0.35	2.1	1.53	28.7	0.92	2.66	**1.44**	1.36	1.06
Small-scale specimens, present study; d = 9.1 in.																				
AP1	U2	39.4	1.85	5190	1/4	1.16	73.2	204	64	15.0	3.8	0.4	3.1	4.31	39.5	0.77	**3.82**	4.04	1.97	1.13
AP2	U2	59.1	2.93	5190	1/4	1.16	73.2	154	29	7.1	1.5	0.3	2.0	2.98	29.6	0.68	3.88	**3.09**	2.11	0.96
AP3	U1	39.4	1.85	5190	1/4	1.16	73.2	37	66	9.8	—	0.5	2.8	4.44	26.4	0.41	4.48	**4.25**	2.62	1.04
AP4	U1	59.1	2.93	5190	1/4	1.16	73.2	83	32	5.9	4.5	0.6	2.2	3.25	18.4	0.53	4.29	**2.89**	2.37	1.12
																			Average	1.16
																			COV	12.7%

*Actual strain is sum of this value and residual plastic strain, which was 4.6×10^{-3}.
†Strut-and-tie capacity governed by second strut.
Notes: 1 in. = 25.4 mm; 145 psi = 1 MPa; 0.145 ksi = 1 MPa; 1 kip = 4.45 kN.

were placed between these base plates and the top steel surface of the reaction beam to minimize longitudinal restraint. The top reaction representing the column force was provided by a bearing plate supported by a roller restrained against longitudinal movement. For Specimen AF11, this plate was 12 x 12 in. (300 x 300 mm) in contact area and was 6 x 12 in. (150 x 300 mm) for the remaining specimens. The three AF intermediate-scale specimens were loaded with the system used for the large-scale specimens using 6 x 12 in. (150 x 300 mm) plates. The TTC specimen in Table 1 was a 46% scale model of a slice of a subway tunnel.[8] It was loaded with seven uniformly spaced loads acting through plates 10.5 x 21.5 in. (265 x 550 mm) in contact area. Although this experiment was conducted to study the shear behavior of a subway tunnel, the loading of the roof slab of the tunnel is very similar to that of the two-column spread footing shown in Fig. 1(c).

DISCUSSION OF EXPERIMENTAL RESULTS

The most important experimental observations from the tests are summarized in Table 1. The definitions of the terms overall length L, tributary shear length L_0, and shear span a are shown in Fig. 4(a). The values of $M/(\rho Vd)$ have been calculated a distance d from the face of the top bearing plate. Experimental results include P, which is the total load applied to the beam at failure, and the parameter $2\Delta/L$, where Δ is the maximum measured vertical displacement. If all of the displacement was caused by shear strain and none by curvature, $2\Delta/L$ would equal the average shear strain. The shear strains γ, which are listed in the table, were measured with pairs of displacement transducers mounted at ± 45 degrees to the horizontal (refer to Fig. 4(b)). By comparing γ with $2\Delta/L$, an assessment of the importance of the shear deformations in causing the total deformations may be made. The maximum diagonal crack widths w, measured at the last load stage prior to failure, are also listed. Finally, the maximum strain measured in the longitudinal reinforcement, ε_s, at the maximum moment location is reported. The strain gauges measuring these strains were set to zero when the applied machine load was zero and hence they did not include the initial compressive strains in the reinforcement caused by concrete shrinkage. The maximum shear at the section d from the face of the top bearings V_d is given in the table in terms of $V_d/(bd\sqrt{f_c'})$.

All specimens failed in shear except AF11 and AP1, which showed signs of flexural yielding prior to failure. No bond failures were observed. Figure 5 shows the crack patterns at failure for many of the specimens in this study. Because all

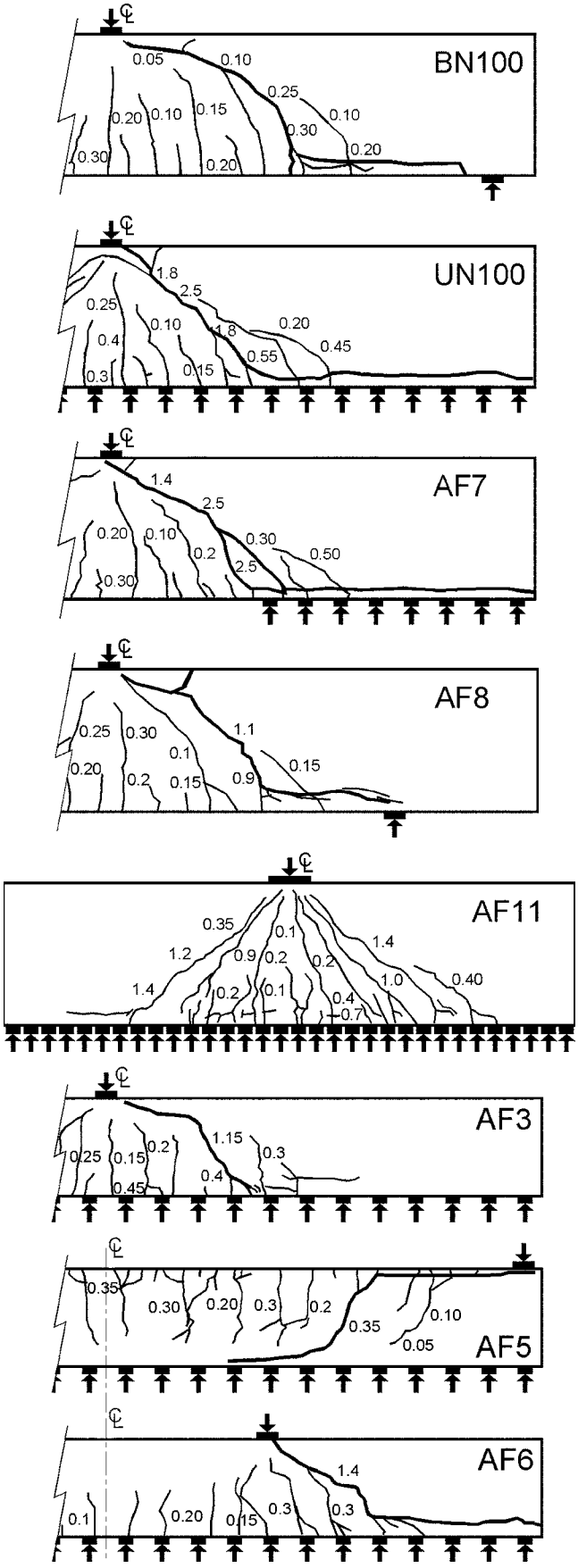

Fig. 5—Observed crack patterns at failure.

specimens were symmetrically loaded, only the half-length of the specimen that contained the failure crack is shown.

It is of interest to compare the failure loads and cracking patterns of the first four large-scale specimens given in Table 1 and shown in Fig. 5. Note that point-loaded member BN100 failed at a shear stress ratio ($V_d/(bd\sqrt{f'_c})$) only approximately 1/2 of that of the companion uniformly loaded Specimen UN100 and that the crack patterns at failure were appreciably different. Specimen AF7 was similar to Specimen UN100, except that the uniform load was not applied near the center of the footing. It is of interest that these two specimens showed very similar failure shear stress ratios and crack patterns, implying that loads applied within d of the column have little influence. The point loads applied to the bottom face of Specimen AF8 are at the same location as the resultant of the uniform loads applied to Specimen AF7; therefore, these two specimens have the same $M/\rho Vd$ ratios at the critical section. In spite of this, Specimen AF7 failed at a shear stress ratio 1.46 times higher than Specimen AF8.

The crack pattern for Specimen AF11 shown in Fig. 5 and the experimental observations in Table 1 were recorded when flexural yielding of the longitudinal reinforcement began. The high shear strains and wide diagonal cracks indicated that a shear failure was imminent. The specimen was unloaded, the jacks in the central region were removed to convert from U1 loading to U1p loading, and the specimen was reloaded as AF11-r. While flexural yielding was now avoided, the maximum allowable oil pressure in the loading system was reached prior to final shear failure of the member.

The crack patterns for three of the intermediate-scale specimens are shown in Fig. 5. Note the very different crack patterns that result from the different loading schemes used. Thus, in Specimen AF3, the flexural cracking is restricted to approximately the central half of the member length, whereas in Specimen AF5, flexural cracking extends for almost the full length. Both specimens failed at very similar loads. Although Specimen AF6 was loaded with two-point loads, the intention of the test was to simulate a U1 footing with a shorter tributary shear length L_0 than Specimen AF3. The crack pattern of this specimen at failure resembles that of Specimens UN100 and AF7 which, like Specimen AF6, had an L_0/d ratio of approximately 3.

The small-scale specimens had depths 1/4 of those of the large-scale specimens and enable a direct comparison to be made of failure shear stress across different depths and slenderness ratios. Figure 6 compares the observed failure shear stress ratios with the effective depth and the slenderness ratios for a large number of the uniformly loaded specimens. It can be seen that there is a substantial decrease in failure shear stress with increasing depth for the slender Shioya[7] tests, where L_0/d equaled approximately 6. For the less slender Toronto experiments with L_0/d of approximately 3, the size effect is much less pronounced. For the even less slender Toronto tests with L_0/d of approximately 2, there is no evidence of a size effect. It is important to note that for most spread footings, the L_0/d ratio will be less than 2.

ANALYTICAL STUDIES

It can be seen that three predicted values of V_d at failure are given in Table 1 for each specimen with the critical one highlighted. The column labeled "Flex" gives the shear corresponding to flexural failure calculated by ACI 318-08.[1] The "Strut" column gives the shear corresponding to crushing of the critical strut calculated using Eq. (5), while

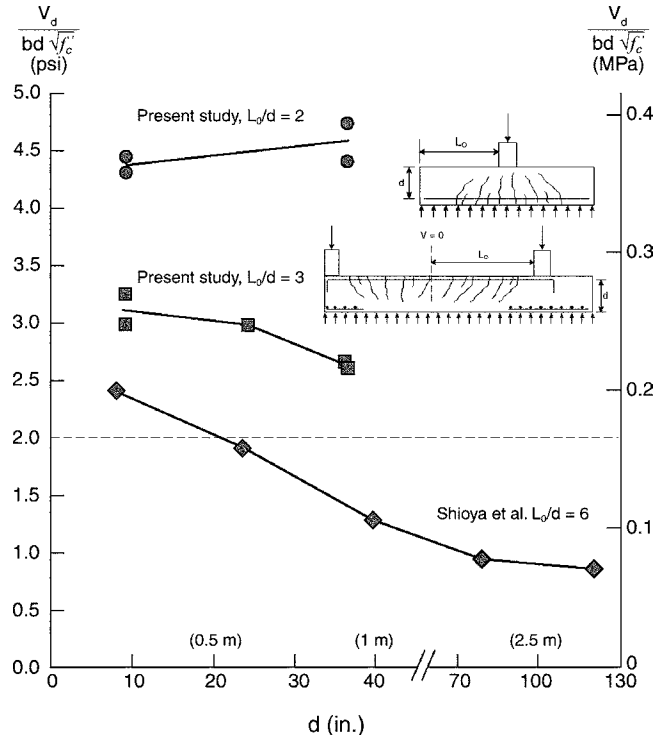

Fig. 6—Observed shear stresses at failure for uniformly loaded members of different depths and different slenderness ratios.

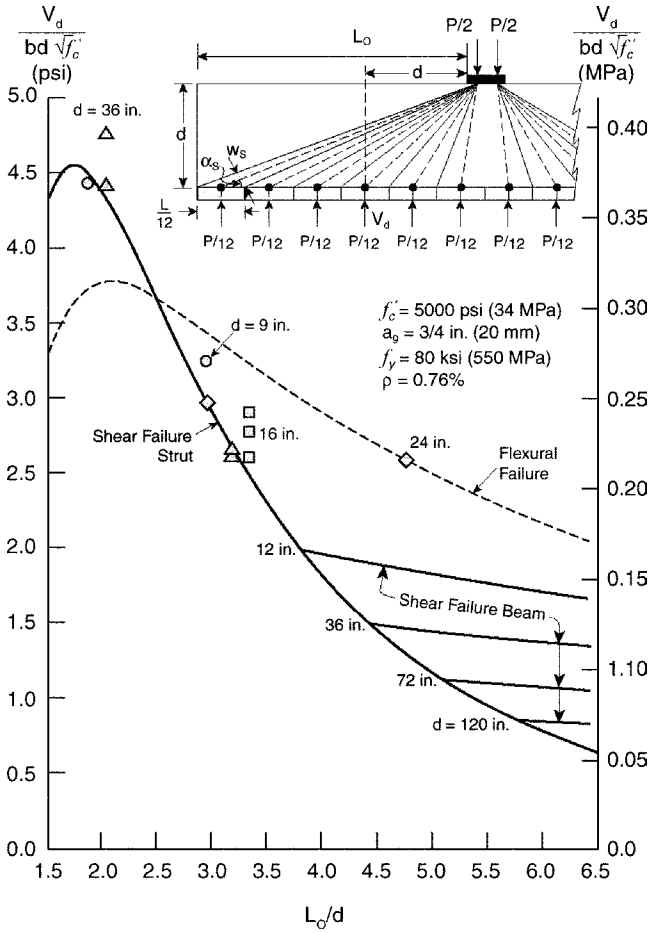

Fig. 7—Predicted and observed failure shears for spread footings.

the values labeled "Beam" correspond to the shear at which the breakdown of beam action is predicted by Eq. (2). As noted with respect to Fig. 3, the predicted shear failure load is the larger of the "Beam" and "Strut" predictions. The predicted failure load, however, cannot exceed the flexural prediction. Also shown in Table 1 are the predicted values of α_s—the calculated strut angle for the optimized strut-and-tie model—and ε_x, the longitudinal strain at middepth calculated by Eq. (4). The strut-and-tie models used for U2 and P loading are shown in Fig. 3, while the strut-and-tie model used for U1 loading is shown in Fig. 7. Overall, the predictions in Table 1 show an average ratio of experimental-to-predicted strength for the 24 specimens as 1.16 with a COV of 12.7%.

In the strut-and-tie model used for U1 loading, 12-point loads along the length of the member were used to represent the uniformly distributed load (refer to Fig. 7). The width of each strut was taken as $(L/12)\sin\alpha_s$—that is, w_t in Eq. (7) is taken as 0 for members with only one layer of reinforcement. The critical strut will be the outer strut with the lowest α_s if there is only one layer of flexural tension reinforcement. If there are multiple layers of reinforcement, the width of the outer strut can be found from Eq. (7). In this case, however, the second strut from the end with the smaller strut width but larger α_s will typically be critical.

The predicted capacity lines shown in Fig. 7 have been prepared for the specific case of 0.76% reinforcement ratio and a concrete strength of 5000 psi (34 MPa). The 12 specimens in Table 1 with reinforcement ratios between 0.68% and 1.16% and U1 or U1p loading have been plotted in the figure. It is important to note from Fig. 7 that although there is a strong size effect predicted for the shear at which beam action breaks down, there is no predicted size effect for failures governed by strut crushing. Thus, for the experimental points plotted at L_0/d of about 3, there is no size effect predicted; however, as shown in Fig. 6, there was in fact a small size effect observed.

It is important to note that the L_0/d ratio below which member depth is predicted to no longer influence failure shear stress depends on the percentage of longitudinal reinforcement, concrete strength, and aggregate size. For an engineer using the convenient ACI 318-08[1] shear strength expression of $2\sqrt{f_c'}\,bd$, which is a simplification of Eq. (1), it is of interest to determine the value of L_0/d below which this equation will be conservative. If the conservative assumptions are that the longitudinal strain ε_s at the critical outside strut is 2×10^{-3}, $\cot\alpha_s$ is L_0/d, and f_c' is 3000 psi (21 MPa), then a shear strength of $2\sqrt{f_c'}\,bd$ will be exceeded when L_0/d is smaller than approximately 2.6.

RECOMMENDED CHANGES TO ACI 318-18[1] CODE

The sectional shear provisions of ACI 318-08[1] neglect the size effect in shear and hence can lead to unconservative estimates of shear capacity for members with large depths. While for beams this safety concern is mitigated by the requirement to provide minimum stirrups if V_u exceeds $0.5\phi V_c$, this provision does not apply to footings. The experimental and analytical results previously presented show that the ACI 318-08[1] procedures can be unconservative for large footings with high slenderness ratios; hence, the exclusion from the minimum shear reinforcement requirements should be limited to footings with low slenderness ratios.

Based on the previous discussion, it can be concluded that the usual ACI 318-08[1] estimate for V_c—namely, $2\sqrt{f_c'}\,bd$—will be conservative for spread footings if the slenderness parameter L_0/d is less than 2.5 regardless of member thickness.

If it is desired to determine the shear capacity of footings with low slenderness ratios more accurately than $2\sqrt{f_c'}\,bd$, then a strut-and-tie model should be formulated and analyzed. It will be found, however, that if ACI 318-08[1] Appendix A is used for this purpose, a discontinuity will be encountered when the angle of the strut drops below 25 degrees. To avoid this discontinuity and obtain more accurate estimates of shear capacity, it is suggested that the 25-degree limit be eliminated and that the effective compressive strength of the concrete strut be taken as

$$f_{ce} = \frac{f_c'}{1.15 + 0.5\cot^2\alpha_s} \tag{8}$$

This equation has been developed from Eq. (5) and (6), assuming that ε_s is approximately 0.002 and that the principal compressive strain in the concrete is somewhat less than the 0.002 conservatively assumed in Eq. (6).

CONCLUDING REMARKS

Reinforced concrete footings are usually constructed without shear reinforcement and often are of substantial thickness. Because ACI 318-08[1] does not account for the size effect in shear, it is possible that large footings designed by this code may be unconservative. Thus, two of the large Japanese footing experiments shown in Fig. 2 failed in shear at less than 50% of the ACI-predicted shear strength. For most footings, however, the loads that generate the shear can be carried by direct strut action and hence the size effect is much less critical. The purpose of this paper is to more clearly identify the footings for which the current ACI 318-08[1] provisions will be unconservative.

This paper summarizes the results of 16 experiments on footing strips, 13 of which were subjected to uniform loads. The shear slenderness of a uniformly loaded member can be defined as L_0/d, where L_0 is the distance from the face of the column or wall to the point of zero shear. For typical spread footings, the traditional ACI 318-08[1] shear provisions are conservative if L_0/d is less than 2.5. When the L_0/d significantly exceeds 3, however, as was the case with the Japanese tests, the ACI 318-08[1] shear provisions can be significantly unconservative (refer to Fig. 6).

This paper also summarizes the results of analytical studies using strut-and-tie models and sectional shear predictions to investigate the shear strength for a range of footing thicknesses, slenderness ratios, and loading types. It is shown that these code-based analytical models are capable of accurately explaining the observed experimental results. It was found that the AASHTO LRFD[20] strut-and-tie model gave better predictions than those of the ACI 318-08[1] Appendix A model. Suggestions are made for improvements to ACI 318-08.[1]

ACKNOWLEDGMENTS

The authors would like to express their gratitude to the Natural Sciences and Engineering Research Council of Canada for a series of grants that made the long-term research project on the shear design of reinforced concrete possible at the University of Toronto.

REFERENCES

1. ACI Committee 318, "Building Code Requirements for Structural Concrete (ACI 318-08) and Commentary," American Concrete Institute, Farmington Hills, MI, 2008, 473 pp.

2. Joint ACI-ASCE Committee 326, "Shear and Diagonal Tension," ACI JOURNAL, *Proceedings* V. 59, No. 1, Jan. 1962, pp. 1-30.

3. Joint ACI-ASCE Committee 326, "Shear and Diagonal Tension," ACI JOURNAL, *Proceedings* V. 59, No. 2, Feb. 1962, pp. 277-334.

4. Joint ACI-ASCE Committee 326, "Shear and Diagonal Tension," ACI JOURNAL, *Proceedings* V. 59, No. 3, Mar. 1962, pp. 352-396.

5. Kani, G. N. J., "How Safe Are Our Large Concrete Beams?" ACI JOURNAL, *Proceedings* V. 64, No. 3, Mar. 1967, pp. 128-142.

6. Bažant, Z. P., and Kim, J.-K., "Size Effect in Shear Failure of Longitudinally Reinforced Beams" ACI JOURNAL, *Proceedings* V. 81, No. 5, Sept.-Oct. 1984, pp. 456-468.

7. Shioya, T., "Shear Properties of Large Reinforced Concrete Member," Special Report of Institute of Technology, Shimizu Corp., No. 25, 1989, 198 pp. (in Japanese)

8. Collins, M. P., and Kuchma, D. "How Safe Are Our Large, Lightly Reinforced Concrete Beams, Slabs, and Footings?" *ACI Structural Journal*, V. 96, No. 4, July-Aug. 1999, pp. 482-490.

9. Richart, F. E., "Reinforced Concrete Wall and Column Footings—Part 1," ACI JOURNAL, *Proceedings*, V. 45, No. 10, Oct. 1948, pp. 97-127.

10. Richart, F. E., "Reinforced Concrete Wall and Column Footings—Part 2," ACI JOURNAL, *Proceedings*, V. 45, No. 11, Nov. 1948, pp. 237-260.

11. Collins, M. P.; Bentz, E. C.; and Sherwood, E. G., "Where is Shear Reinforcement Required? Review of Research Results and Design Procedures," *ACI Structural Journal*, V. 105, No. 5, Sept.-Oct. 2008, pp. 590-600.

12. Sherwood, E. G.; Bentz, E. C.; and Collins, M. P., "The Effect of Aggregate Size on the Beam-Shear Strength of Thick Slabs," *ACI Structural Journal*, V. 104, No. 2, Mar.-Apr. 2007, pp. 180-190.

13. Bentz, E. C.; Vecchio, F. J.; and Collins, M. P., "Simplified Modified Compression Field Theory for Calculating Shear Strength of Reinforced Concrete Elements," *ACI Structural Journal*, V. 103, No. 4, July-Aug. 2006, pp. 614-624.

14. Vecchio, F. J., and Collins, M. P., "The Modified Compression Field Theory for Reinforced Concrete Elements Subjected to Shear," ACI JOURNAL, *Proceedings* V. 83, No. 2, Mar.-Apr. 1986, pp. 219-231.

15. CSA A23.3-04, "Design of Concrete Structures," Canadian Standards Association, Mississauga, ON, Canada, 2004, 214 pp.

16. Kani, G. N. J., "The Riddle of Shear Failure and Its Solution," ACI JOURNAL, *Proceedings*, V. 61, No. 4, Apr. 1964, pp. 441-468.

17. Leonhardt, F., and Walther, R., "The Stuttgart Shear Tests, 1961," Cement and Concrete Association Library Translation No. 111, Dec. 1964, 134 pp. (translated into English from a collection of articles that appeared in *Beton und Stahlbetonbau*, V. 56, No. 12, 1961, and V. 57, No. 2, 3, 6, 7, and 8, 1962)

18. Krefeld, W. J., and Thurston, C. W., "Studies of the Shear and Diagonal Tension Strength of Simply Supported Reinforced Concrete Beams," ACI JOURNAL, *Proceedings*, V. 63, No. 4, Apr. 1966, pp. 451-476.

19. Kani, G. N. J., "Basic Facts Concerning Shear Failure," ACI JOURNAL, *Proceedings*, V. 63, No. 6, June 1966, pp. 675-692.

20. AASHTO LRFD, "Bridge Design Specifications and Commentary," third edition, American Association of State Highway Transportation Officials, Washington, DC, 2004, 1264 pp.

21. Collins, M. P.; Mitchell D.; and Bentz E. C., "Shear Design of Concrete Structures," *The Structural Engineer*, V. 86, No. 10, May 2008, pp. 32-39.

22. Uzel, A., "Shear Design of Large Footings," PhD thesis, Department of Civil Engineering, University of Toronto, ON, Canada, 2003, 383 pp.

23. Angelakos, D.; Bentz, E. C.; and Collins, M. P., "Effect of Concrete Strength and Minimum Stirrups on Shear Strength of Large Members," *ACI Structural Journal*, V. 98, No. 3, May-June 2001, pp. 290-300.

Disc. 108-S13/From the March-April 2011 *ACI Structural Journal*, p. 131

Design of Large Footings for One-Way Shear. Paper by Almila Uzel, Bogdan Podgorniak, Evan C. Bentz, and Michael P. Collins

Discussion by Andor Windisch

ACI member, PhD, Karlsfeld, Germany

The experimental program and analytical studies using strut-and-tie models presented in the paper pose some questions:

- The data shown in Table 1 reveal that only the depths of the specimens were chosen systematically. All other characteristics form a stochastic cloud; thus, any statistical evaluation is misleading, even though the average and coefficient of variation (COV) are quite comforting.
- It is prudent to refer to the slabs of Richart[9,10]; nevertheless, the type of loading resulting from uniformly distributed springs or hydraulic jacks, respectively, results in fundamentally different failure patterns. Due to the deformation of the specimens during loading, the springs near the ends of the footings bear less and less of the load. This is why the Exp./Pred. ratios listed in Table 1 are significantly higher than the case of the other specimens. Hence, they should not be considered in the statistical evaluation.

Discussing the experimental results, the authors write: "All specimens failed in shear except AF11 and AP1, which showed signs of flexural yielding prior to failure. No bond failures were observed." The crack patterns shown in Fig. 5 clearly contradict this statement. Specimens BN100, UN100, AF7, AF8, AF5, and AF6 show pronounced horizontal cracks along the line of the flexural reinforcement, which result in the softening of the bond, increasing the crack width of the critical section and resulting in failure. For the same reason, the strains measured in the longitudinal reinforcement at the maximum moment location, ε_s, are irrelevant.

During the analytical studies, the authors look for the "optimized critical" strut, which—for U1 loaded specimens—is the last strut shown in Fig. 7, or in the case of Specimen AF13, the second to last nearby. The governing geometrical size of the struts is their width w_s calculated with Eq. (7). Nevertheless, comparing the relevant crack patterns shown in Fig. 5 with the strut pattern shown in Fig. 7 reveals that the specimens are completely uncracked in these regions. Moreover, when calculating the predicted shear failures of the spread footings, the authors neglect the second term of Eq. (7), hence diminishing the corresponding Exp./Pred. values and "improving" the average and COV values. The authors should clarify for designers under which conditions which terms of their now fairly empirical model can be omitted. It is astonishing to see in Fig. 7 that the widest width of the strut governs its strength and not the very narrow opposite end under the loading plate. Please clarify.

Studying the experimental results and comparing them with the results of the analytical studies, it is interesting to learn that one of the shortest specimens, AF11, failed in flexure. Please clarify. How was this possible?

For the other specimens with U1-type loading, three specimens with L_0/d of approximately 3 were predicted to fail in flexure—five in strut shear and four in beam shear (Specimen AF3 with L_0/d = 4.74 in beam shear and Specimen UN100 with L_0/d = 3.16 in strut shear). Nevertheless, the crack patterns shown in Fig. 5 are identical for all of these specimens. What is the mechanical background for the different predictions? Please clarify.

Looking at Eq. (2) to (4), which are based on the modified compression field theory (MCFT), the following comments can be made:

- The effective crack spacing (Eq. (3)) is not influenced by the maximum aggregate size or the effective depth but by the bond characteristics of the longitudinal reinforcement, which is not considered.
- Most of the crack patterns shown in Fig. 5 also completely contradict Eq. (3). The crack governing the failure was the last one—that is, no crack spacing can be deduced there.
- Neither the maximum diagonal crack widths w listed in Table 1 nor the relative crack widths w/d show any correspondence to the given Exp./Pred. values. This reveals that the source of the shear capacity is not the aggregate interlock; hence, the validity of Eq. (3) must be questioned as well.
- It is questionable whether MCFT-based equations could be applied at all in the case of these footings, as the original Toronto test panels showed—at least in one direction—a dense reinforcement. These test specimens had some tensile longitudinal reinforcing bars only and high regions of the web were unreinforced.

The failure stress of the diagonal strut calculated according to Eq. (5) and (6), which is based on the MCFT,[14] does not have any mechanical relevance. The principal tensile strain ε_1 in the concrete perpendicular to the strut should be compatible with the uncracked concrete in the large regions around the critical strut. Moreover, as the authors correctly state, in the case of uniformly loaded beams (Type U2), the critical section is near the support, where the moment is low. How does this fit into Eq. (5) and (6)?

Calculating the average values for the three groups of Toronto specimens, it is interesting that the mean values for the large-, intermediate-, and small-scale specimens are 1.08, 1.23, and 1.06, respectively, which reveals that Eq. (2) to (6) preferred by the authors have a systematic deviation in the case of d = 24 in. (~0.60 m). Please clarify.

The authors state that the threshold value of L_0/d between the strut and beam depends on the percentage of longitudinal reinforcement, concrete strength, and aggregate size (which is questionable). As a simplification, they propose that L_0/d equals approximately 2.5 to 2.6. Then, recalculating the angle of the (last) strut, one arrives at approximately 25 degrees; hence, the introduction of smaller angles as proposed by the authors is not necessary. Thus, the effective compressive strength of the concrete strut, as proposed in Eq. (8), which does not have any real

mechanical or theoretical background (note the uncracked concrete regions), becomes irrelevant as well.

AUTHORS' CLOSURE

Table 1 presents nine different variables that describe the specimens in this paper. To systematically vary these nine variables over four different values (as was presented for depth) would require a total of 4^9 tests. Thus, to satisfy the discusser, a total of 262,144 shear tests would have been required rather than the 24 tests shown in Table 1. Clearly, this is not realistic. The statistical evaluations in the paper were performed in an identical manner to those performed in the calibration of code equations, the evaluation of public safety, and so on.

The authors disagree that Richart[9,10] did a poor job of applying uniform loads to his experimental footing slabs of the 1940s. The method used was to force the slab to displace into a bed of relatively low stiffness springs. By using low stiffness springs, the individual spring displacements would be fairly consistent, as members failing in shear are stiff. What matters for the nonuniformity of the load would be the nonuniformity of the displacements, and this would have been small.

The crack patterns shown in Fig. 5 were based on the appearance of the specimens after they failed and after the load was removed. In a number of cases, the dowel action of the flexural reinforcing bars resulted in the bottom cover being pushed off the specimen after failure occurred. (This was confirmed with high-speed video recording.) Thus, some of the pictures in Fig. 5 show what appear to be extensive bond cracking, but this occurred after the load resisted by the specimen was already decreasing; thus, this could not have been the trigger of failure.

The discusser needs to recall that the strut-and-tie method is a lower-bound method. It need not be the case that the final crack diagrams match the assumed model in every detail. The strut-and-tie model used for Fig. 7 is the one that is predicted to produce the lowest strength; thus, this was the one that was used. Given that the code does not allow uncracked concrete tension ties, it is not clear to the authors what other strut-and-tie model could have been used to carry the load from the footing to the column in the absence of stirrups.

The strut-and-tie model used for the analysis of the U1 specimens is shown in Fig. 7. The uniform loading is simulated in the figure with a set of 12 concentrated loads. For the 10 "inner" fan struts, which go from the "soil" up to the top column load, it is clear from the geometry that only the first part of Eq. (7) can be used, as it would be geometrically impossible for both terms of the equation to apply. For simplicity, it is recommended that all struts be treated this way, except for cases where there are multiple layers of longitudinal reinforcement. In such cases, as for Specimen AF13, this strut will generally not control; the second strut, which does not have this second term, will control instead.

The discusser is surprised that the authors have taken the critical location in the strut-and-tie model in Fig. 7 as the wide end rather than the narrow end of the strut. This is clearly explained on page 133 of the original paper, which notes: "As Eq. (5) indicates that the strut strength will be lowest where the tensile straining is greatest, the calculated critical strength in the strut will be that calculated at the flexural tension side of the member."

The discusser asks how Specimen AF11—the shortest specimen—could have failed in flexure rather than shear. Figure 3 clearly shows that as beams get shorter, the predicted shear strength increases rapidly. If the span is sufficiently short, flexural failures will result. This, of course, is one of the key conclusions of Kani[5] in terms of a "valley of diagonal failure," whereby sufficiently long or sufficiently short members will not fail in shear. Specimen AF11 was on the edge of the valley of shear failure. The paper combined three different predicted failure modes: 1) sectional shear failure; 2) strut-and-tie shear failure; and 3) flexural failure. The first was governed by the breakdown of the ability to resist aggregate interlock, the second by the inability of a strut to carry compression across cracked concrete, and the third by the maximum ability of steel to resist tension stresses. When the span lengths are varied, different failure modes are predicted to govern, as shown in Fig. 7. The mechanical background for these methods is presented in the paper and need not be repeated herein. The lack of perfect matching between crack diagrams and strut-and-tie models is discussed previously.

With regard to the influence of member depth and aggregate size on effective crack spacing, the discusser is encouraged to follow up on References 7 and 12, both of which are clearly cited in the original paper.

Figure 5 highlights the failure shear crack with a darker line. At the level of the flexural tension reinforcement, none of the critical cracks were "the last," as the discusser claims. It should also be noted that the methods in this paper are not intended to predict crack patterns but instead shear strengths, and Table 1 shows that they do this rather well.

The largest observed crack width in a beam will result from many different factors. The discusser seems to believe that there should be a numerical correlation between the observed maximum crack width and the ability of the MCFT-based shear methods to predict shear strength. This appears to be an attempt to compare apples to oranges, as one should not expect there to be a correlation such as this.

The discusser asks whether or not the MCFT-based methods in this paper can be applied to footings. Table 1 shows that the methods do indeed work well, with an average test-to-predicted ratio of 1.16 with a COV of only 12.7%.

The equations used to determine the average principal tensile strain in the concrete strut result from a Mohr's circle of strain. The authors believe that this is an appropriate way to determine strain transformations. Equations (5) and (6) apply equally to "disturbed regions" near supports and regions away from supports. In the authors' opinion, no special guidance for the application of these equations is needed.

The discusser notes that the different-sized specimens have different average test-to-predicted ratios. This is due to natural experimental scatter and is not surprising. The higher average for the intermediate scale specimens noted by the discusser is primarily a result of Test AF3, which was unusually strong compared to the predictions.

Note that the proposed solution for when engineers can ignore the size effect for footings is indeed that these footings need only receive special attention when the L_0/d ratio is larger than approximately 2.5. This was chosen as a convenient simplification and is not intended to be a replacement for the strut-and-tie method in the ACI code.

Plastic Hinge Lengths in High-Rise Concrete Shear Walls. Paper by Alfredo Bohl and Perry Adebar

Discussion by Himat Solanki and Sonal Thakkar

ACI member, Sarasota, FL, and Assistant Professor, Nirma University, Ahmedabad, India

The authors have presented an interesting paper on empirical equations for plastic hinge lengths in high-rise concrete shear walls considering the size effect; however, the discussers would like to offer the following comments:

1. Table 1 does not address whether the loading condition is monotonic or cyclic because the plastic hinge length varies with the loading condition.

2. The values of $\varphi_{max,1}$ and $\varphi_{max,2}$ specified in Eq. (10) are unclear. Are these values at a 2% drift or an ultimate curvature ductility? If they are based on the ultimate curvature ductility or a 2% drift, what was the value of displacement or curvature ductility and what was the relationship between the curvature ductility and displacement ductility?

Based on the published literature, φ_y is related to ε_y and φ_{max} and φ_u are related to the displacement ductility or curvature ductility.

3. The authors' Eq. (9) refers to the term *z*. Because the neutral axis depth associated with the maximum curvature value φ_{max} could be approximated to $0.2l_w$, and if $0.1l_w$ is a clear cover of reinforcement in each side of the wall, the value of *z* would be approximately $0.833l_w$. By substituting $z = 0.833l_w$ in Eq. (9), Eq. (9) would become

$$l_p = \left(0.2l_w + 0.05(0.833l_w)\right)\left(1 - 1.5P / f_c'A_g\right) \le 0.8l_w \quad (11)$$

If $P/f_c'A_g = 0$, then l_p would be

$$l_p = 0.242l_w \quad (12)$$

This value is inconsistent with References 2 and 22.

4. Because the plastic hinge length l_p is a hypothetical length over which the maximum curvature is assumed to be constant,[31] the conservative estimates of the plastic hinge length would be[22]

$$l_p = \left(0.2 + 0.044A_r\right)l_w \quad (13)$$

where A_r is the aspect ratio h_w/l_w of the wall.

Equation (13) does not consider the $P/f_c'A_g$ term. Based on the typical uniform distribution of reinforcement, including the edge boundary element effects,[18,22,31] the $P/f_c'A_g$ term could be introduced in Eq. (13) and the plastic hinge length would be

$$l_p = \left(0.2 + 0.044A_r\right)l_w\left(1 - 1.3P / f_c'A_g\right) \le 0.8l_w \quad (14)$$

If l_w = 12.5 ft (3.81 m), h_w = 180 ft (54.86 m), and $P/f_c'A_g$ = 0.30, then l_p = 6.36 ft (1.94 m) in lieu of the authors' value of 6.3 ft (1.93 m).

If l_w = 25.0 ft (7.62 m), h_w = 180 ft (54.86 m), and $P/f_c'A_g$ = –0.05, then l_p = 13.76 ft (4.19 m) in lieu of the authors' value of 15.0 ft (4.59 m).

If l_w = 25.0 ft (7.62 m), h_w = 180 ft (54.86 m), and $P/f_c'A_g$ = 0.0, then l_p = 12.9 ft (3.93 m) in lieu of the authors' value of 14.0 ft (4.27 m).

Considering the values of Eq. (9), Eq. (14) is in good agreement with the hinge length specified in Table 1 with a 0 to 8% (+/–) variation.

REFERENCES

31. Park, R., and Paulay, T., *Reinforced Concrete Structures*, John Wiley & Sons, Inc., New York, 1975, 769 pp.

AUTHORS' CLOSURE

The authors appreciate the interest in their paper. The following are in response to the specific comments/questions.

1. The subject of the paper is plastic hinge lengths in concrete shear walls subjected to seismic (reverse cyclic) bending. Reverse cyclic loading increases plastic hinge lengths because of additional cracking and bond slip that occurs during load cycles. In the nonlinear finite element analysis that was done to develop the results given in Table 1, the influence of reverse cyclic loading was captured using appropriately reduced concrete tension stresses (tension-stiffening model). The model was validated by comparing predictions with tests of walls subjected to reverse cyclic loading (Fig. 1 and 2).

2. If two parallel shear walls with different lengths l_{w1} and l_{w2} are interconnected only at the top, the wall with the longer horizontal dimension l_{w1} would yield first at a smaller top displacement because the yield curvature of a wall is inversely proportional to the wall length. This hypothetical case was used to formulate a displacement-based design approach for shear wall buildings.[32] In real buildings, parallel shear walls are interconnected at many points over the building height by floor slabs; this results in a complex interaction between walls of different lengths. When walls are interconnected at numerous points, it is not possible for the longer wall to develop a plastic hinge while the other wall is still elastic because the two walls must maintain the same deformed shape. Both walls will yield at essentially the same top wall displacement.

The relationship between displacement and curvature in two parallel walls with different lengths is essentially controlled by the longer wall, except in the plastic hinge zone of the more slender wall. As discussed in the paper, the height over which inelastic curvatures spread in a shear wall depends on the wall length. Thus, the more slender wall will have a smaller zone of inelastic curvature but must have the same deflected shape above the plastic hinge zones—the two walls must have the same inelastic rotation. The result of this is that the more slender wall will have significantly larger maximum inelastic curvature demands at the base (Fig. 8(a) and 11).

Equation (10) in the paper provides an estimate of the larger maximum curvature demand $\phi_{max,2}$ in the wall with the smaller horizontal dimension l_{w2} and thus smaller equivalent plastic hinge length $l_{p,2}$ and smaller yield curvature $\phi_{y,2}$,

given the maximum curvature demand $\phi_{max,1}$ in the wall with the larger horizontal dimension l_{w1} and thus larger equivalent plastic hinge length $l_{p,1}$ and larger yield curvature $\phi_{y,1}$. Equation (10) can be used to estimate the maximum curvature demand in the more slender wall at any drift level at which the walls are yielding. The first step is to determine the relationship between the particular building drift and maximum curvature demand $\phi_{max,1}$ in the longer wall, using an appropriate relationship for a single wall.[3,5] The previously suggested methods for estimating curvature demand from curvature ductility and displacement ductility relationships are strongly discouraged.[5] The ratio of plastic hinge lengths $l_{p,1}/l_{p,2}$ in Eq. (10) can be determined by applying Eq. (9) or a simplified version of Eq. (9) (discussed in the following) to each of the walls. The final two parameters in Eq. (10)—the yield curvatures of the two walls $\phi_{y,1}$ and $\phi_{y,2}$—can be estimated very simply as $0.003/l_{w1}$ and $0.003/l_{w2}$.

3. The parameter z that appears in seven of the eight equations presented in the paper for estimating equivalent plastic hinge length, including Eq. (9) developed by the authors, is clearly defined in the paper as the bending moment-to-shear ratio M/V or the distance from the maximum-to-zero bending moment. The discussers appear to use an estimate of the internal flexural lever arm to arrive at a nonsensical value for z. The actual values of z will never be that small and will often be 10 times larger.

4. Equation (13) was discussed in the paper and was compared with the nonlinear analysis results in Fig. 7(c).* Equation (13) does not predict the nonlinear analysis results very well because it does not account for the level of axial compression force. Presumably, the impetus for combining Eq. (13) with the authors' proposed Eq. (9) is to account for the axial compression without the parameter z. The most appropriate way to eliminate z is to estimate the relationship between $z = M/V$ and wall height h_w. As described in the paper, Eq. (7) was developed by assuming $z = h_w$; however, a more refined estimate can easily be made. If the hinging at the base of a shear wall is due to a first-mode distribution of forces, the ratio M/V at the base of the wall will be approximately $0.7h_w$. This value of z would be appropriate for flexural walls in lower-height buildings (for example, 10 stories tall). The maximum curvatures at the base of a shear wall in a taller building (for example, 30 stories tall) are strongly influenced by higher modes, such as the second mode; thus, a lower value of z should be used (for example, $0.4h_w$). The need to use a range of z/h_w values for different-height buildings is why Eq. (9) was not simplified, as suggested by the discussers.

REFERENCES

32. Priestley, M. J. N.; Calvi, M. C.; and Kowalsky, M. J., *Displacement-Based Seismic Design of Structures*, IUSS Press, Pavia, Italy, 2007, 670 pp.

*Editor's note: For convenience, below is the corrected figure as provided by the author. The corrected figure has been replaced in the PDF version of the original paper, which is available online at **www.concrete.org**.

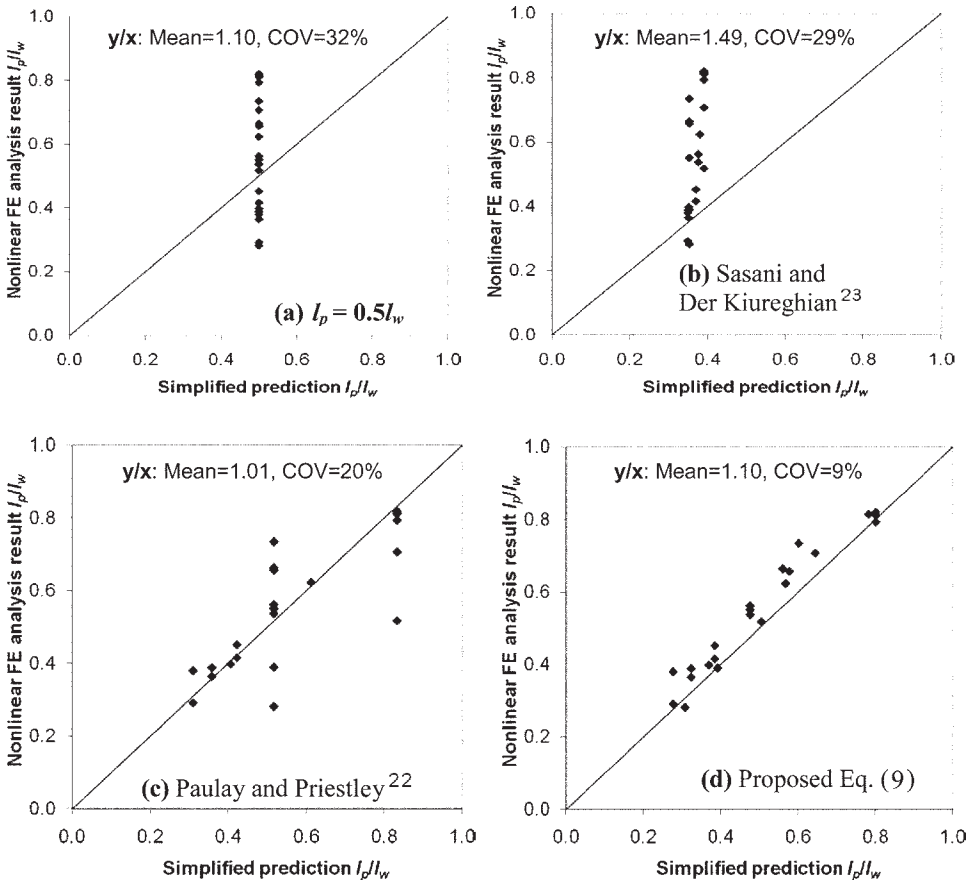

Fig. 7—Comparison of l_p/l_w determined from nonlinear finite element analysis and simplified procedures.

Disc. 108-S17/From the March-April 2011 *ACI Structural Journal*, p. 167

Shear Deformations of Slender Reinforced Concrete Walls under Seismic Loading. Paper by Katrin Beyer, Alessandro Dazio, and M. J. Nigel Priestley

Discussion by Shiming Chen and Kang Ge

Professor, School of Civil Engineering, Tongji University, Shanghai, China, and Research Student, School of Civil Engineering, Tongji University

The discussers appreciate the authors' comprehensive work to analyze and evaluate the shear deformations in rectangular and nonrectangular reinforced concrete (RC) walls derived from the available quasi-static cyclic tests. The significance of the development of shear deformation in the plastic hinge zones is analyzed and assessed. A simplified estimation of the expected shear deformations in walls controlled by flexure was proposed, which could be a supplement to deformation computation using normal inelastic beam elements. Some findings are interesting to the discussers and worthy of further discussion.

SHEAR MECHANISMS

Whereas flexural members are subjected to inelastic reversing, cyclic rotations' shear deformation may be expected to develop in the plastic hinge zone, which leads to a large part of the stiffness degradation.[34,35] For calculation of the top displacement that corresponds to flexural yielding, the deformation in the web-shear mechanism should also be considered, together with the deformation in the flexural mechanism.

In RC shear walls subjected to seismic loads, the flexural mechanism—both web shear and sliding shear—would be activated. These two shear deformations have high values, even in the case where the structural elements are designed to exhibit flexural behavior. It was found that in shear walls with a low aspect ratio, sliding shear deformations appear at the base plastic hinge, even in the case where the flexural behavior initially predominates the response. The displacement at the top of the walls due to the deformation of the sliding shear mechanism at the base of these walls was found to be significantly increased after the displacement ductility reached 2.5.[36] Hence, for the calculation of the top displacement ductility, the deformation of all load-resisting mechanisms, such as the flexural and shear mechanisms of the two, should be taken into account.

Sliding shear displacements were not considered for the typical wall designs in the paper. It is not clear if the typical design was adopted for all walls studied or just for the U-shaped walls. The aspect ratio of the shear walls varies from 2.0 to 4.0 and no special joint detailing is illustrated. Can the authors demonstrate what detailing or criterion was used for these typical walls, where the sliding shear deformation can be neglected?

For the calculation of the displacement ductility, the contribution of the shear mechanisms to the top displacement should be added to the inelastic deformations after yield. Does the ductility demand adopted in the analysis include the contribution of the shear deformation?

AXIAL STRAINS' DISTRIBUTION OVER CROSS SECTION

Figure 4 shows the distribution of shear and axial strains for U-shaped Wall TUA at a certain ductility level when the lateral loads are exerted parallel to the web (Position A). It appears that although the shear force is kept the same, the shear deformation is not evenly distributed. It varies along the wall height, and the magnitude of the shear deformation depends not only on the shear force but also on the inelastic flexural deformations.

The discussers wonder how the axial strains were captured in the tests. Were they captured by strain gauges or by the Demec measurements at the side surface of the wall? The axial strains illustrated by the gray shaded areas do not distribute uniformly across the cross sections of the U-shaped wall along the wall height, even at a place far beyond the plastic hinge region, as it appears. Because the axial load was kept the same during the tests, the developed axial strains should contribute by the lateral force. It is not clearly explained and understood that the west flange has a very small axial strain (tensile strain?), whereas the east flange develops a larger axial strain (compressive strain?). At the lower section near the plastic region, however, both the west and east flanges were subjected to the (compressive) axial strain but with different magnitudes.

The cross sections of the U-shaped wall do not remain plane at the deflection ductility of 3.0 or even less. The axial strain distributions likely suggest that the U-shaped wall distorts warping. It is also not clear whether the lateral force parallel to the web acted through the shear center of the U-shaped section. Otherwise, the shear deformation contributed from the twisting force would be included.

Can the authors clarify whether similar distortions and strains occurred in the other rectangular section RC walls?

SHEAR-TO-FLEXURAL DISPLACEMENT RATIOS

It has been verified that the response of low-aspect-ratio walls differs significantly from the response of RC walls with aspect ratios over 2.0.[36] The shear force that corresponds to diagonal cracking in a low-aspect-ratio wall has a lower value than the shear force that corresponds to flexural cracking, whereas slender RC walls—for example, with aspect ratios greater than 2.0 or 3.0—behave in a ductile flexural mode other than shear failure when loaded beyond the elastic limit.

Figure 6 shows the variation of Δ_s/Δ_f ratios with top drift for cantilever RC walls tested under cyclic loading. It appears that the walls with shear-controlled behavior (PCA Phases I and II) developed a drift ratio of 3%, whereas the capacity-designed RC walls[11] developed less drift. Axial load should contribute to improve the ductile performance of shear walls. The shear deformation and associated stiffness degradation develop progressively as inelastic cyclic rotations are applied to a hinge zone. Because a drift ratio of 3% is a very large value of interstory deformation, it will typically accompany a severe drop in the load resistance of the structure. Which shear-to-flexural displacement ratios are expected at a typical, accepted drift ratio—say, 1% or even less?

The shear-to-flexural displacement ratios vary considerably between the walls. As the ratio of shear-to-flexural displacement remains approximately constant over the entire ductility range in the RC walls governed by flexure and with

a stable shear-transfer mechanism, a simple model for estimating the Δ_s/Δ_f ratios was proposed. In the case of a wall with a degrading shear-transfer mechanism, however, the shear-to-flexural displacement ratio increases with ductility demand and Δ_s/Δ_f is also strongly dependent on the loading history. It would be interesting to develop a simple rule or have a criterion to distinguish between these two differently behaving walls in design practice.

REFERENCES

34. Fenwick, R. C., "Shear Deformation in Seismic Frame Structures," *Journal of Structural Engineering*, ASCE, V. 109, No. 4, 1983, pp. 965-976.

35. Aristizabal-Ochoa, J. D., "Cracking and Shear Effects on Structural Walls," *Journal of Structural Engineering*, ASCE, V. 109, No. 5, 1983, pp. 1267-1277.

36. Salonikios, T. N., "Analytical Prediction of the Inelastic Response of RC Walls with Low Aspect Ratio," *Journal of Structural Engineering*, ASCE, V. 133, No. 6, 2007, pp. 844-854.

AUTHORS' CLOSURE

The authors thank the discussers for their interest in the paper on shear deformations of slender RC walls. The issues raised will be commented on in the order presented in the discussion.

SHEAR MECHANISMS

1. The discussers state that the top displacement that corresponds to flexural yielding should also consider the shear deformation. The authors agree with the discussers on this point. The computation of the yield displacement was not a subject of the paper, however, but is covered elsewhere.[37]

2. The discussers point out the importance of sliding deformations for squat walls. For slender walls, which are the subject of the paper, the authors' own experimental results[7,11,13] have, however, shown that sliding deformations constitute only a relatively minor part of the total deformations. For the U-shaped walls, for example, the sliding deformations were measured at the base of the web and flanges and the sliding displacements contributed between 2 to 5% to the total top displacements.[7] The shear deformations in the Δ_s/Δ_f ratio comprise both the shear deformations of the wall and the sliding displacements along the joint between the wall and foundation. The authors agree with the discussers that the design for sliding shear resistance requires additional research and found that some design guidelines for sliding shear can lead to very conservative designs requiring diagonal reinforcement.[7] None of the walls that were included in the database of the paper, however, featured diagonal reinforcement.

3. The discussers wonder whether the ductility demand adopted in the analysis includes shear deformations. The displacement ductility μ was computed for total deformations, which is standard practice—that is, it included flexural and shear deformations.

AXIAL STRAINS' DISTRIBUTION OVER CROSS SECTION

1. The discussers note that the shear deformations are not only related to the shear force but also vary over the height of the wall. This is correct and was discussed at length in the paper. The shear deformations are, for example, also a function of the axial strains caused by flexural deformations, which are not constant over the height of the wall.

2. The discussers wonder how the axial strains shown in Fig. 4(a) were captured in the tests. Similar to the shear strains, the axial strains were obtained from Demec measurements (refer to the legend in Fig. 4(a)).

3. The discussers observe that the axial strains are not uniformly distributed over the wall section, particularly above the plastic hinge zone. The authors assume that the discussers expected a linear distribution of strains. The photos of the U-shaped test[7] units show that the crack spacing in the upper part of the wall was larger than the base length of the vertical Demec measurements (200 mm [7.87 in.]). For this reason, the Demec measurements do not result in linear strain profiles.

4. The discussers wonder about the axial strain distribution shown in Fig. 4(a). The tensile axial strains are plotted above the line representing the midheight of the Demec measurement length, whereas the compression strains are plotted below this line. At Position A (Fig. 1(b)), the compression zone lies in the west flange. It should be noted, however, that the compression zone depth is smaller than the flange thickness. Because the Demec measurements were taken on the inside faces of the wall, the axial strains of the west flange at Position A are also positive but, of course, are considerably smaller than the axial strains in the east flange.

5. The discussers state that it does not become clear whether the actuator force parallel to the web acted through the shear center of the U-shaped section. The purpose of this paper was not to explain in detail the test setup for the U-shaped wall tests—the test setup, loading history, boundary condition, and so on are published elsewhere.[7] It is recalled herein, however, that twisting of the top of the U-shaped wall was prevented throughout the test, with the only exception of selected load steps, where the torsional stiffness of the wall was explicitly investigated. The shear center of an RC U-shaped wall subjected to inelastic deformations is not at a constant distance to the web. With increasing inelastic deformations, the shear center moves closer to the web.[7]

SHEAR-TO-FLEXURAL DISPLACEMENT RATIOS

1. The discussers state that "slender RC walls…behave in a ductile flexural mode other than shear failure, when loaded beyond the elastic limit." The authors disagree with this statement and point out that slender RC walls can also fail in shear.

2. The discussers wonder what Δ_s/Δ_f ratio is expected at drift ratios of 1% or less. The authors point out that the question is answered by Fig. 6, which shows the Δ_s/Δ_f ratios for drift values between 0.2% and failure. Moreover, an important finding of the paper is that "for walls forming a flexural hinge and a stable shear-transfer mechanism, the ratio of shear-to-flexural displacement remains approximately constant over the entire ductility range once the walls have reached their nominal strength" (refer to the conclusions of the paper). Equation (8) for estimating the Δ_s/Δ_f ratio is therefore applicable to the entire ductility range.

3. The discussers propose the development of a simple rule for differentiating between walls that are failing in flexure and walls that are failing in shear. The purpose of the paper was not to develop new equations for the flexural and shear resistance of RC walls but instead to study the deformation components of slender RC walls. Strength equations that allow for the estimation of whether a flexural or shear failure occurs are included in all structural design codes.

REFERENCES

37. Dazio, A.; Beyer, K.; and Bachmann, H., "Quasi-Static Cyclic Tests and Plastic Hinge Analysis of RC Structural Walls," *Engineering Structures*, V. 31, No. 7, 2009, pp. 1556-1571.